Modular Construction of $A_{1+x}M_{4-2x}M'_{7+x}Se_{15}$ (A = K, Rb; M = Pb, Sn; M′ = Bi, Sb): A New Class of Solid State Quaternary Thermoelectric Compounds

Kyoung-Shin Choi,[†] Duck-Young Chung,[†] Antje Mrotzek,[†] Paul Brazis,[‡] Carl R. Kannewurf,[‡] Ctirad Uher,[§] Wei Chen,[§] Tim Hogan,[||] and Mercouri G. Kanatzidis*[,†]

Department of Chemistry and Center for Fundamental Materials Research, Michigan State University, East Lansing, Michigan 48824, Department of Electrical Engineering and Computer Science, Northwestern University, Evanston, Illinois 60208, Department of Physics, University of Michigan, Ann Arbor, Michigan 48109, and Department of Electrical and Computer Engineering, Michigan State University, East Lansing, Michigan 48824

Received April 21, 2000. Revised Manuscript Received December 6, 2000

Five isostructural compounds, $K_{1.25}Pb_{3.5}Bi_{7.25}Se_{15}$ (**I**), $K_{1.46}Sn_{3.09}Bi_{7.45}Se_{15}$ (**II**), $Rb_{1.45}Pb_{3.1}Sb_{7.45}Se_{15}$ (**III**), $K_{1.45}Pb_{3.1}Sb_{7.45}Se_{15}$ (**IV**), and $K_{2.15}Pb_{1.7}Sb_{8.15}Se_{15}$ (**V**) were prepared by the molten flux method as silver rodlike air-stable crystals. They all crystallize in the monoclinic space group $P2_1/m$ with $a = 17.4481(8)$ Å, $b = 4.1964(2)$ Å, $c = 21.695(1)$ Å, $\beta = 98.850(1)°$ for **I**, $a = 17.454(5)$ Å, $b = 4.201(1)$ Å, $c = 21.760(6)$ Å, $\beta = 98.550(5)°$ for **II**, $a = 17.3160(7)$ Å, $b = 4.1406(2)$ Å, $c = 21.6401(8)$ Å, $\beta = 99.139(1)°$ for **III**, $a = 17.1204(6)$ Å, $b = 4.1568(2)$ Å, $c = 21.6362(8)$ Å, $\beta = 98.706(1)°$ for **IV**, and $a = 17.167(4)$ Å, $b = 4.1494(9)$ Å, $c = 21.684(5)$ Å, $\beta = 98.664(3)°$ for **V** ($Z = 2$ for all compounds). The general formula $A_{1+x}M_{4-2x}M'_{7+x}Se_{15}$ (A = K, Rb; M = Pb, Sn; M′ = Bi, Sb) is derived from a large degree of variability in composition that is expressed in terms of mixed occupancy among A^+, M^{2+}, and M'^{3+} atoms. The structure type has a three-dimensional framework assembled from NaCl- and Bi_2Te_3-type modular units. The framework features narrow tunnels filled with K^+/Rb^+ ions. The NaCl- and Bi_2Te_3-type units are composed of edge-shared distorted Bi^{3+}/Sb^{3+} octahedra. The Pb/Sn atoms are stabilized in 8-coordinated bicapped trigonal prismatic sites at the connecting points of NaCl-type blocks and Bi_2Te_3-type blocks. There exists a considerable amount of occupancy disorder among Pb/Sn, Bi/Sb, and K/Rb in the structure. $K_{1.25}Pb_{3.5}Bi_{7.25}Se_{15}$ is a potential new thermoelectric material with high power factor and low thermal conductivity at room temperature. The electrical conductivity and the thermopower for several $A_{1+x}M_{4-2x}M'_{7+x}Se_{15}$ phases are reported. The optical band gaps were determined to be 0.53 (**I**), 0.39 (**II**), 0.36 (**III**), 0.45 (**IV**), and 0.60 (**V**) eV at room temperature. The compounds seem to melt congruently at 685 (**I**), 662 (**II**), 578 (**III**), 576 (**IV**), and 576 (**V**) °C.

1. Introduction

Several new concepts that relate structure and thermoelectric (TE) properties are stimulating renewed interest and research activity in thermoelectric materials.[1−5] The challenge in finding a superior TE material lies in achieving high electrical conductivity (σ), high thermopower (S), and low thermal conductivity (κ) in the same material. These properties define the TE figure of merit $ZT = (\sigma \cdot S^2/\kappa) \cdot T$. Our approach to compounds with a high figure of merit has been to search for new semiconducting multinary bismuth chalcogenide materials. Specifically, we target incorporating alkali and alkaline earth metal ions into infinite anionic metal-chalcogen frameworks. These ions are stabilized between the layers or in the channels of the anionic framework, making relatively weak ionic bonds with chalcogens, and act as "rattlers" in their local cavities. These rattlers create low-frequency vibration modes that scatter acoustic phonons and, thus, reduce the thermal conductivity. Other factors contributing to low

* To whom correspondence should be addressed.
[†] Department of Chemistry and Center for Fundamental Materials Research, Michigan State University.
[‡] Northwestern University.
[§] University of Michigan.
[||] Department of Electrical and Computer Engineering, Michigan State University.

(1) *Thermoelectric Materials-New Directions and Approaches*; Kanatzidis, M. G., Lyon, H., Mahan, G., Tritt, T., Eds.; *Mater. Res. Soc. Symp. Proc.*, **1997**, *478*, references therein. (b) *Thermoelectric Materials--The Next Generation Materials for Small-Scale Refrigeration and Power Generation Applications*; Tritt, T., Lyon, H., Jr., Mahan, G., Kanatzidis, M., Eds.; *Mater. Res. Soc. Symp. Proc.* **1999**, *545*, references therein.

(2) (a) Slack, G. A. New Materials and Performance Limits for Thermoelectric Cooling. In *CRC Handbook of Thermoelectrics*; Rowe, D. M., Ed.; CRC Press: Boca Raton, FL, 1995; pp 407−440. (b) Slack, G. A. *Solid State Physics*; Ehrenreich, H., Seitz, F., Turnbull, D., Eds.; Academic: New York, 1997; Vol. 34, p 1.

(3) (a) Sales, B. C. *Mater. Res. Bull.* **1998**, *23*, 15−21. (b) Sales, B. C.; Mandrus, D; Williams, R. K. *Science* **1996**, *272*, 1325−1328. (c) Sales, B. C.; Mandrus, D; Chakoumakos, B. C.; Keppens, V.; Thompson, J. R. *Phys. Rev. B* **1997**, *56*, 15081−15089.

(4) Tritt, T. M. *Science* **1996**, *272*, 1276−1277.

(5) (a) Chung, D.-Y.; Iordanidis, L.; Choi, K.-S.; Kanatzidis, M. G. *Bull. Korean Chem. Soc.* **1998**, *19*, 1283−1293. (b) Kanatzidis, M. G. *Semicond. Semimet.* **2000**, in press.

10.1021/cm0003323 CCC: $20.00
Published on Web 02/10/2001

thermal conductivity in materials are the presence of heavy atoms (e.g., Bi, Pb), large unit cells, and mass fluctuation disorder in the crystal lattice. The compounds $BaBiTe_3$,[6] β-$K_2Bi_8Se_{13}$,[7] $K_{2.5}Bi_{8.5}Se_{14}$,[7] $CsBi_4Te_6$,[8] $K_2Bi_8S_{13}$,[9] and $KBi_{6.33}S_{10}$[9] exhibit promising TE properties, encouraging us to look into more complex quaternary systems. The structural complexity in these materials can produce corresponding complexities in the electronic band structure, which according to the Mott formula[10] could give rise to high thermopower coupled with high electrical conductivity.

To further explore the effects of structural complexity and mass fluctuation in compounds with large unit cells, we began to investigate quaternary systems by incorporating Pb metal to the K/Bi/Se system. In addition to being very heavy, Pb has similar electronic properties to Bi and has a well-known tendency to disorder with Bi or alkali metals, depending on the local coordination environment.[11−13] Site occupancy disorder in the structure generates randomness of the mass, size, and charge of the atoms on a particular lattice position that can strongly scatter acoustic lattice phonons carrying heat.[2]

These investigations led to new families of quaternary solids, such as the $K_{1+x}M_{4-2x}Bi_{7+x}Se_{15}$ (M = Pb, Sn), $A_{1-x}M_{4-x}Bi_{11+x}Se_{21}$,[14] (A = K, Rb, Cs), and $K_{1-x}Pb_{5-x}Bi_{11+x}Se_{22}$.[15] The corresponding Sb analogues of $K_{1+x}M_{4-2x}Bi_{7+x}Se_{15}$ are also stable. The structure types associated with these classes are new and a remarkable characteristic of them all is the extensive mixed occupancy of certain crystallographic sites between K, M, and Bi (or Sb) atoms. This property has two important consequences: first, it generates a continuum of isostructural compositions with varying band gaps, and second, it sets the stage for systems with very low thermal conductivity. The former is advantageous because it provides a mechanism for controlling the electrical properties of these materials, whereas the latter is a necessary condition for any viable TE material. Therefore, certain members of this, apparently large, class of isostructural compounds may hold high potential for TE applications. We report here the syntheses, structures, and physicochemical and thermoelectric properties of the members, $K_{1.25}Pb_{3.5}Bi_{7.25}Se_{15}$, $K_{1.46}Sn_{3.09}Bi_{7.45}Se_{15}$, $Rb_{1.45}Pb_{3.1}Sb_{7.45}Se_{15}$, $K_{1.45}Pb_{3.1}Sb_{7.45}Se_{15}$, and $K_{2.15}Pb_{1.7}Sb_{8.15}Se_{15}$. We show that $K_{1.25}Pb_{3.5}Bi_{7.25}Se_{15}$ is in fact a promising TE candidate material.

2. Experimental Section

2.1. Synthesis. The following reagents were used as obtained: lead metal, 99.999%, 200 mesh, Cerac, Milwaukee, WI; tin metal, 99.999%, 200 mesh, Cerac, Milwaukee, WI; bismuth selenide, 99.999% −325 mesh, Cerac, Milwaukee, WI; antimony, −200 mesh, Cerac, Milwaukee, WI; selenium powder, 99.5+%, 100 mesh, Aldrich Chemical Co., Milwaukee, WI or selenium shots, 99.999%, Noranda Advanced Materials, Quebec, Canada; rubidium metal, 99.8%, Johnson Matthey Co., Ward Hill, MA; potassium metal, rod 99.5% purity, Aldrich Chemical Co., Milwaukee, WI. The starting materials K_2Se and Rb_2Se were prepared by a stoichiometric reaction of potassium/rubidium metal with selenium in liquid NH_3. M_2Se_3 (M = Bi, Sb) was prepared by heating a stoichiometric mixture of bismuth or antimony and selenium at 750 °C for 48 h.

$K_{1.25}Pb_{3.5}Bi_{7.25}Se_{15}$, $Rb_{1.45}Pb_{3.1}Sb_{7.45}Se_{15}$, and $K_{1.45}Pb_{3.1}Sb_{7.45}Se_{15}$. The compounds were synthesized from a mixture of 2 mmol of A_2Se (A = K or Rb), 2 mmol of Pb, 3 mmol of M_2Se_3 (M = Bi or Sb), and 10 mmol of Se. The reagents were thoroughly mixed, sealed in an evacuated Pyrex tube, and heated at 540 °C for 5 days (cooling rate of 2 °C/h). Isolation in degassed dimethylformamide (DMF) and water gave pure silver-colored needles of each compound (yield >95% based on Pb). The crystals are air- and water-stable. A quantitative microprobe analysis with a SEM/EDS system, performed on different crystals, gave the average compositions $K_{1.2}Pb_{3.5}Bi_{7.3}Se_{14.8}$, $Rb_{1.35}Pb_{3.3}Sb_{7.48}Se_{15.1}$, and $K_{1.55}Pb_{3.1}Sb_{7.5}Se_{15}$.

$K_{2.15}Pb_{1.70}Sb_{8.15}Se_{15}$. The compound was prepared from a mixture of 4 mmol of K_2Se, 1 mmol of Pb, 3 mmol of Sb_2Se_3, and 10 mmol of Se using the same synthetic conditions as described above. EDS/SEM analysis gave $K_{2.2}Pb_{1.73}Sb_{8.3}Se_{15.3}$.

$K_{1.46}Sn_{3.09}Bi_{7.45}Se_{15}$. This compound was discovered from the reaction of an amount of 1 mmol of K_2Se, 4 mmol of Sn, 3 mmol of Bi_2Se_3, and 4 mmol of Se. The mixture (thoroughly mixed) was sealed in an carbon-coated silica tube and heated at 900 °C for 6 h, followed by cooling to room temperature at a rate of 100 °C/h. A shiny silver ingot of the pure phase was obtained after isolation in dimethylformamide (DMF) and washing with methanol and diethyl ether. Single crystals of $K_{1.46}Sn_{3.09}Bi_{7.45}Se_{15}$ were prepared when the reaction mixture was heated at 800 °C for 120 h and slowly cooled at a rate of 10 °C/h. The silver ribbonlike crystals were obtained by isolation in degassed DMF and washed with methanol and ether. The crystals are air- and water-stable. After the stoichiometry was determined by both EDS analysis and X-ray crystallographic refinement (see below), the compound could be prepared from the stoichiometric proportions of K_2Se/Sn/Bi_2Se_3/Se, that is, 0.75 mmol/3 mmol/3.75 mmol/3 mmol, respectively.

It was difficult to determine the exact formulas for the Sb phases based only on the X-ray crystallographic refinement due to sites in the structure with considerable mixed occupancy among K^+/Rb^+, Pb^{2+}, and Sb^{3+}. We cannot exclude triply disordered sites in these compounds. Therefore, all the formulas are based on taking collectively into account (a) elemental analyses obtained by electron microprobe energy-dispersive spectroscopic (EDS) analysis, (b) crystallographically refined composition (except when Pb/Bi differentiation is involved, see below), and (c) a requirement of charge neutrality. The EDS-determined compositions were adjusted to the nearest charge-balanced formula.

2.2. Physical Measurements. Electron Microscopy. Quantitative microprobe analyses of the compounds were performed with a JEOL JSM-35C SEM equipped with a Tracer Northern EDS detector. Data were acquired using an accelerating voltage of 25 kV and a 60-s accumulation time. The quantitative microprobe analyses have a standard deviation of about 4−6%. Typically, an average of three to four measurements were taken from each crystal.

Infrared Spectroscopy. Optical diffuse reflectance measurements were made on the finely ground sample at room temperature. The spectrum was recorded in the infrared region (6000−400 cm^{-1}) with the use of a Nicolet MAGNA-IR 750

(6) Chung, D.-Y.; Jobic, S.; Hogan, T.; Kannewurf, C. R.; Brec, R.; Rouxel, J.; Kanatzidis, M. G. *J. Am. Chem. Soc.* **1997**, *119*, 2505−2515.

(7) Chung, D.-Y.; Choi, K-.S; Iordanidis, L.; Schindler, J. L.; Brazis, P.; Kannewurf, C. R.; Chen, B.; Hu, S.; Uher C.; Kanatzidis, M. G. *Chem. Mater.* **1997**, *9*, 3060−3071.

(8) Chung, D.-Y.; Hogan, T.; Brazis, P. W.; Rocchi-Lane, M.; Kannewurf, C. R.; Bastea, M.; Uher, C.; Kanatzidis, M. G. *Science* **2000**, *287*, 1024−1027.

(9) (a) Kanatzidis, M. G.; McCarthy, T. J.; Tanzer, T. A.; Chen, L.-H.; Iordanidis, L.; Hogan, T.; Kannewurf, C. R.; Uher, C.; Chen, B. *Chem. Mater.* **1996**, *8*, 1465−1474.

(10) *CRC Handbook of Thermoelectrics*; Rowe, D. M., Ed.; CRC Press, Inc.: Boca Raton, FL, 1995, and references therein.

(11) Takagi, J.; Takéuchi, Y. *Acta Crystallogr.* **1972**, *B28*, 649−651.

(12) Takéuchi, Y.; Takagi, J. *Proc. Jpn. Acad.* **1974**, *50*, 76−79.

(13) Skowron, A; Boswell, F. W.; Corbett, J. M.; Taylor, N. J. *J. Solid State Chem.* **1994**, *112*, 307−311.

(14) Mrotzek, A.; Chung, D.-Y.; Ghelani, N.; Hogan, T.; Kanatzidis, M. G. *Chem. Eur. J.* **2001**, in press.

(15) Mrotzek, A.; Chung, D.-Y.; Hogan, T.; Kanatzidis, M. G. *J. Mater. Chem.* **2000**, *10*, 1.

Table 1. Summary of Crystallographic Data and Structure Analysis.

formula[a]	$K_{1.25}Pb_{3.5}Bi_{7.25}Se_{15}$	$K_{1.46}Sn_{3.09}Bi_{7.45}Se_{15}$	$Rb_{1.45}Pb_{3.1}Sb_{7.45}Se_{15}$	$K_{1.45}Pb_{3.1}Sb_{7.45}Se_{15}$	$K_{2.15}Pb_{1.7}Sb_{8.15}Se_{15}$
F.W.[a]	3473.54	3165.14	2857.66	2790.42	2612.95
crystal habit	silver needles	silver ribbons	silver needles	silver needles	silver needles
space group	$P2_1/m$	$P2_1/m$	$P2_1/m$	$P2_1/m$	$P2_1/m$
a, Å	17.4481(8)	17.454(5)	17.3160(7)	17.1204(6)	17.164(4)
b, Å	4.1964(2)	4.201(1)	4.1406(2)	4.1568(2)	4.1494(9)
c, Å	21.6945(10)	21.750(6)	21.6401(8)	21.6362(8)	21.684(5)
β, °	98.8500(10)	98.550(5)	99.1390(10)	98.706(1)	98.664(3)
Z, V, Å^3	2, 1569.54(13)	2, 1577.2(8)	2, 1531.87(11)	2, 152202(11)	2, 1527.0(6)
$D_{calc,}$[a] g/cm^3	7.350	6.665	6.195	6.089	5.683
temp, K	293(2)	293(2)	171(2)	171(2)	293(2)
λ(Mo Kα), Å	0.71069				
μ(Mo Kα),[a] cm^{-1}	767.31	622.13	435.29	417.05	345.88
$F(000)$[a]	2845	2621	2396	2343	2212
θ_{max}, deg	28.30	28.47	28.84	28.35	28.70
total data measd	12085	12486	10198	10547	12322
unique data	4208 ($R_{int} = 0.0821$)	3948 ($R_{int} = 0.0592$)	4089 ($R_{int} = 0.0427$)	3992 ($R_{int} = 0.0546$)	3992 ($R_{int} = 0.0433$)
no. of variables	166	175	174	166	165
refinement method	full-matrix least-squares on F^2				
final R indices [$I > 2\sigma$]	R1[b] = 0.0537 wR2[c] = 0.1126	R1 = 0.0625 wR2 = 0.1469	R1 = 0.0432 wR2 = 0.0931	R1 = 0.0533 wR2 = 0.1095	R1 = 0.0502 wR2 = 0.1308
GOF on F^2	0.921	1.161	0.994	1.029	1.043

[a] Formula, formula weight, D_{calc}, μ, and $F(000)$ are based on the formula proposed by EDS analysis. [b] $R1 = \sum||F_o| - |F_c||/\sum|F_o|$. [c] $wR2 = \{\sum[w(F_o^2 - F_c^2)^2]/\sum[w(F_o^2)^2]\}^{1/2}$.

Spectrometer equipped with a Collector Diffuse Reflectance of Spectra-Tech. Inc. The reflectance versus wavenumber data were used to estimate a material's band gap by converting reflectance to absorption data as described previously.[16]

Differential Thermal Analysis (DTA). DTA experiments were performed on a computer-controlled Shimadzu DTA-50 thermal analyzer. Typically, a sample (≈20 mg) of ground crystalline material was sealed in silica tubes under vacuum. A silica tube of equal mass filled with Al_2O_3 was sealed and placed on the reference side of the detector. The samples were heated to 800 °C at 5 °C/min and isothermed for 10 min, followed by cooling at −5 °C/min to 50 °C. Residues of the DTA experiments were examined by X-ray powder diffraction. The stability of the samples was monitored by running multiple heating/cooling cycles.

Charge-Transport Measurements. dc electric conductivity and thermopower measurements were made on single crystals of the compounds. Conductivity measurements were performed in the usual four-probe geometry with 60- and 25-μm gold wires used for the current and voltage electrodes, respectively. Measurements of the sample cross-sectional area and voltage probe separation were made with a calibrated binocular microscope. Conductivity data were obtained with the computer-automated system described elsewhere.[17] Thermoelectric power measurements were made by using a slow ac technique[15,18] with 60-μm gold wires serving to support and conduct heat to the sample as well as to measure the voltage across the sample resulting from the applied temperature gradient. In both measurements, the gold electrodes were held in place on the sample with a conductive gold paste.

Conductivity specimens were mounted on interchangeable sample holders, and thermopower specimens were mounted on a fixed sample holder/differential heater. Mounted samples were placed under vacuum (10^{-3} Torr) and heated to room temperature for 2−4 h to cure the gold contacts. For a variable-temperature run, data (conductivity or thermopower) were acquired during both sample cooling and warming to check reversibility. The temperature drift rate during an experiment was kept below 1 K/min. Typically, three to four separate variable-temperature runs were carried out for each sample to ensure reproducibility and stability. At a given temperature, reproducibility was within ±5%.

Thermal Conductivity Measurements. Thermal conductivity was determined using a longitudinal steady-state method over the temperature range 4−300 K. The samples were attached (using either a low melting point solder or silver-loaded epoxy) to the cold tip of the cryostat, while the other end of the samples were provided with a small strain gauge resistor (thin film) which serves as a heater. The temperature differences across the samples were measured using a differential chromel−constantan thermocouple.

2.3. X-ray Crystallography. A single crystal of each compound was mounted on the tip of a glass fiber. Intensity data were collected on a Siemens SMART Platform CCD diffractometer using graphite monochromatized Mo Kα radiation over a full sphere of reciprocal space. The individual frames were measured with an omega rotation of 0.3° and an acquisition time of 45 s per frame. The SMART software[19] was used for the data acquisition and SAINT[20] for data extraction and reduction. The absorption correction was done using SADABS.[21] Structure solution and refinement for all compounds were performed with the SHELXTL package[22] of crystallographic programs. All compounds are isostructural and were solved and refined successfully in the $P2_1/m$ space group. The complete data collection parameters, details of the structure solution, and the refinement for each compound are given in Table 1.

$K_{1.25}Pb_{3.50}Bi_{7.25}Se_{15}$. Because Pb^{2+} and Bi^{3+} have similar atomic weights and scattering power, resolution between them is impossible by X-ray diffraction. Nominally, the 8-coordinate sites were assigned as Pb(1) and Pb(2) and the 6-coordinate sites as Bi(1)−Bi(9) because in the analogues with Sb or Sn the M^{2+} mainly occupies the 8-coordinate sites and M'^{3+} occupies the 6-coordinate sites. After successive refinements, the atomic displacement parameters (ADPs) for the Pb(1) and Pb(2) remained high, indicating that these sites should be disordered with the lighter K atoms. The occupancy refinement shows that the Pb(1) and Pb(2) sites contain 10.9(6)% of K(1′) and 14.3(6)% of K(2′), respectively. The octahedral Bi sites had

(16) McCarthy, T. J.; Ngeyi, S.-P.; Liao, J.-H.; Degroot, D.; Hogan, T.; Kannewurf, C. R.; Kanatzidis, M. G. *Chem. Mater.* **1993**, *5*, 331−340.

(17) Lyding, J. W.; Marcy, H. O.; Marks, T. J.; Kannewurf, C. R. *IEEE Trans. Instrum. Meas.* **1988**, *37*, 76−80.

(18) Chaikin, P. I.; Kawk, J. F. *Rev. Sci. Instrum.* **1975**, *46*, 218−220.

(19) *SMART*; Siemens Analytical X-ray Systems, Inc.: Madison, WI, 1994.

(20) *SAINT: Version 4*; Siemens Analytical X-ray Systems, Inc.: Madison, WI, 1994−1996.

(21) *SADABS: Area-Detector Absorption Correction*; Siemens Analytical X-ray Systems, Inc.: Madison, WI, 1996.

(22) *SHELXTL: Version 5*; Siemens Analytical Xray Systems, Inc.: Madison, WI, 1994.

Table 2. Fractional Atomic Coordinates and Equivalent Atomic Displacement Parameter (U_{eq}) Values for $K_{1.25}Pb_{3.50}Bi_{7.25}Se_{15}$ with Estimated Standard Deviations in Parentheses[a]

atoms	*x*	*y*	*Z*	U_{eq},[b] Å^2
Pb(1)/K(1′)[c]	0.3300(1)	1/4	0.7735(1)	0.020(1)
Pb(2)/K(2′)[d]	0.7769(1)	1/4	0.6832(1)	0.019(1)
Bi(1)[e]	0.4546(1)	1/4	0.1669(1)	0.011(1)
Bi(2)	0.7563(1)	1/4	0.8799(1)	0.011(1)
Bi(3)	0.0340(1)	1/4	0.0928(1)	0.014(1)
Bi(4)	0.1848(1)	1/4	0.9413(1)	0.013(1)
Bi(5)	0.6063(1)	1/4	0.0266(1)	0.013(1)
Bi(6)	0.0535(1)	1/4	0.7146(1)	0.012(1)
Bi(7)	0.3253(1)	1/4	0.4814(1)	0.010(1)
Bi(8)	0.0681(1)	1/4	0.4323(1)	0.011(1)
Bi(9)	0.8064(1)	1/4	0.3938(1)	0.010(1)
K(1)	0.5069(4)	1/4	0.6328(3)	0.018(2)
Se(1)	0.4619(2)	1/4	0.9036(1)	0.015(1)
Se(2)	0.3207(2)	1/4	0.0454(1)	0.010(1)
Se(3)	0.8937(2)	1/4	0.9855(1)	0.011(1)
Se(4)	0.5705(2)	1/4	0.2659(1)	0.011(1)
Se(5)	0.6255(2)	1/4	0.7802(1)	0.011(1)
Se(6)	0.1761(2)	1/4	0.1839(1)	0.014(1)
Se(7)	0.430(2)	1/4	0.8476(1)	0.015(1)
Se(8)	0.7373(2)	1/4	0.1190(1)	0.013(1)
Se(9)	0.3350(2)	1/4	0.3565(1)	0.014(1)
Se(10)	0.0684(2)	1/4	0.3059(1)	0.010(1)
Se(11)	0.8231(2)	1/4	0.2711(1)	0.011(1)
Se(12)	0.5711(2)	1/4	0.4922(1)	0.010(1)
Se(13)	0.8149(2)	1/4	0.5511(1)	0.011(1)
Se(14)	0.575(2)	1/4	0.5788(1)	0.009(1)
Se(15)	0.3016(2)	1/4	0.6274(1)	0.011(1)

[a] The composition of $K_{1.25}Pb_{3.50}Bi_{7.25}Se_{15}$ was obtained from EDS analysis and was slightly adjusted to the nearest charge-balanced formula. [b] U_{eq} is defined as one-third of the trace of the orthogonalized U_{ij} tensor. [c] 89.1(6)% Pb(1) and 10.9(6)% K(1′). [d] 85.7(6)% Pb(2) and 14.3(6)% K(2′). [e] The Bi sites contain varying amounts of Pb.

reasonable ADPs and did not display any mixed occupancy with K atoms. Once the amount of K^+ ions in the compound was determined, the ratio of Pb^{2+} and Bi^{3+} could be calculated under the assumption that the compound is valence precise (i.e., no mixed valency). The resulting final formula $K_{1.25}Pb_{3.50}Bi_{7.25}Se_{15}$ is in good agreement with that proposed by elemental analysis (SEM/EDS). Table 2 gives the final atomic coordinates of this structure type. The labeling scheme is the same for all compounds and the corresponding tables for the remaining compounds are given in the Supporting Information.

$K_{1.46}Sn_{3.09}Bi_{7.45}Se_{15}$. An analytical absorption correction using the program XPREP [22] was followed by a semiempirical absorption correction based on symmetrically equivalent reflections that was done for each data set with the program SADABS.[21] The structure refinement revealed relatively high thermal displacement parameters for the Bi(1)−(6), Bi(8)−(9), and Sn(1)−(2) sites, which introduced a disorder model with mixed Bi/Sn and Sn/K occupancies, respectively, for these sites. The refinement resulted in 12% Sn in the Bi(1) site, 17% Sn in the Bi(2) site, 33% Sn on the Bi(3) site, 26% Sn in the Bi(4) site, 29% Sn on the Bi(5) site, 7% Sn in the Bi(6) site, 21% Sn on the Bi(8) site, 11% Sn on the Bi(9) site, 30% K on the Sn(1) site, and 15% K on the Sn(2) site. After successive refinements a prominent peak (6.09 e Å^{-3}) in the electron density map was found 0.79 Å away from the Sn(2) site, so the K(2′) site was moved to this position to introduce positional disorder between Sn(2) and K(2′). The final formula $K_{1.46}Sn_{3.09}Bi_{7.45}Se_{15}$ is charge-balanced within the standard deviation of the occupancies, which is in acceptable agreement with "$K_{1.77}Sn_{2.98}Bi_{7.66}Se_{15}$" obtained from EDS. The selected bond distances for $K_{1.25}Pb_{3.50}Bi_{7.25}Se_{15}$ and $K_{1.46}Sn_{3.09}Bi_{7.45}Se_{15}$ are given in Table 3.

$Rb_{1.45}Pb_{3.1}Sb_{7.45}Se_{15}$. Unlike $K_{1.25}Pb_{3.5}Bi_{7.25}Se_{15}$ for which we practically dealt with the disorder between only two species (K and indistinguishable Pb/Bi), here there are three distinguishable elements, Rb, Sb, and Pb. For the sites with abnormally high ADPs, we introduced occupancy disorder. For example, the Pb(2) site with a high ADP (U_{eq} = 0.026 Å^2) can be disordered with lighter Rb and/or Sb but this site was arbitrarily disordered with only Rb, which resulted in 82.1(5)% Pb/17.9(5)% Rb with a lowered ADP (U_{eq} = 0.021 Å^2). Among the Sb sites, Sb(3), Sb(4), and Sb(6) had lower ADPs, indicating mixed occupation with heavier Pb atoms. The refinement resulted in 29.4(8)%, 27.3(7)%, and 19.9(7)% of Pb in Sb(3), Sb(4), Sb(6) sites, respectively. The resulting formula $Rb_{1.18}Pb_{2.59}Sb_{8.23}Se_{15}$ is not charge-balanced, assuming Rb^+, Pb^{2+}, Sb^{3+}, and Se^{2-}. We cannot exclude the possibility that the other Sb sites with reasonable ADPs may also be disordered with heavier Pb and lighter Rb at the same time in such ratios that the ADPs remain reasonable. If a site is occupied by three different atoms, mathematically there is more than one way to assign partial occupancy for each element so that the resulting calculated scattering electron density for the site is the same as the observed one. In addition, when we refined occupancies for more than three triply disordered sites under the constraint of charge balance, the refinement became unstable and diverged. Therefore, the Rb/Pb/Sb ratio was determined from the elemental analysis results provided by EDS.

$K_{1.45}Pb_{3.1}Sb_{7.45}Se_{15}$. The 8-coordinate Pb(1) and Pb(2) sites once again had high ADPs and mixed occupation with 9.2(4)% of K(1′) and 29.4(5)% of K(2′). Because the ADPs for the Sb atoms were normal, a Pb contribution was not considered for these sites. However, the EDS results require more Pb content than the total Pb amount suggested by the refinement for the 8-coordinate sites, implying that the Sb sites may have varying contributions from both Pb and K atoms.

$K_{2.15}Pb_{1.7}Sb_{8.15}Se_{15}$. Both Pb(1) and Pb(2) sites showed high ADPs. For the Pb(1) site, introducing mixed occupancy did not drop the ADPs and the amount of K atom refined for this site was negligible. This indicated that the high ADPs for the Pb(1) site was mainly due to the positional fluctuation so-called "rattling effect" of the Pb atoms in this large pocket. The Pb(2) site was refined to 50.5(5)% Pb/49.5(5)% K. The difference in the total Pb content in the 8-coordinate sites for both $K_{1.45}Pb_{3.1}Sb_{7.45}Se_{15}$ and $K_{2.15}Pb_{1.7}Sb_{8.15}Se_{15}$ are not significant. Therefore, the difference should lie in the Pb amount disordered with Sb on the octahedral sites. The composition $K_{2.15}Pb_{1.7}Sb_{8.15}Se_{15}$, indicated by EDS/SEM, contains only half of the Pb present in $K_{1.45}Pb_{3.1}Sb_{7.45}Se_{15}$. The selected bond distances for $K_{1.45}Pb_{3.1}Sb_{7.45}Se_{15}$ and $K_{2.15}Pb_{1.7}Sb_{8.15}Se_{15}$ are given in Table 4.

3. Results and Discussion

Structure. The structural motif associated with the $A_{1+x}M_{4-2x}M'_{7+x}Se_{15}$ (A = K, Rb; M = Pb, Sn; M′ = Bi, Sb) family is shown in Figure 1. This is an anisotropic three-dimensional monoclinic structure, which propagates along the *b* axis with the very short repeating length of ≈4.2 Å. In fact, this is a persistent feature of all ternary or quaternary bismuth and antimony chalcogenide compounds and it is responsible for their highly anisotropic needlelike crystal growth habits. All atoms are situated on crystallographic mirror planes lying perpendicular to the *b* axis.

The three-dimensional "$M_{4-2x}Bi_{7+x}Se_{15}$" framework is assembled from two different structural modules, both of which are infinite along the *b* axis. The first is a stepped layer having the thickness and structural features of a Bi_2Te_3-type layer. These stepped layers are parallel to the *ab* plane; see Figure 1. The second structural element, which is also found in β-$K_2Bi_8Se_{13}$ and $K_{2.5}Bi_{8.5}Se_{14}$,[7] is an infinite rod, which can be regarded as an excised block from the NaCl lattice. In the cross section, the rod is rectangular and 3-Bi octahedra × 2-Bi octahedra wide. These so-called 3 × 2 rods, indicated in Figure 1, serve as pillars between the

Table 3. Selected Distances (Å) for $K_{1.25}Pb_{3.5}Bi_{7.25}Se_{15}$ and $K_{1.46}Sn_{3.09}Bi_{7.45}Se_{15}$

	$K_{1.25}Pb_{3.5}Bi_{7.25}Se_{15}$	$K_{1.46}Sn_{3.09}Bi_{7.45}Se_{15}$		$K_{1.25}Pb_{3.5}Bi_{7.25}Se_{15}$	$K_{1.46}Sn_{3.09}Bi_{7.45}Se_{15}$
M(1)−Se(4) ×2	2.934(2)	2.838(3)	M(2)−Se(9) ×2	2.905(2)	2.830(3)
M(1)−Se(15)	3.133(3)	3.023(5)	M(2)−Se(13)	3.038(3)	2.999(5)
M(1)−Se(1)	3.355(3)	3.502(5)	M(2)−Se(10) ×2	3.399(3)	3.519(3)
M(1)−Se(11) ×2	3.418(3)	3.562(4)	M(2)−Se(6) ×2	3.559(3)	3.605(4)
M(1)−Se(8) ×2	3.473(3)	3.703(4)	M(2)−Se(5)	3.622(3)	3.749(4)
Bi(1)−Se(4)	2.715(3)	2.696(3)	Bi(6)−Se(7)	2.920(3)	2.970(3)
Bi(1)−Se(5) ×2	2.857(2)	2.847(2)	Bi(6)−Se(14)	2.958(3)	2.904(2)
Bi(1)−Se(1) ×2	3.091(2)	3.132(2)	Bi(6)−Se(10) ×2	2.972(2)	2.963(2)
Bi(1)−Se(2)	3.241(3)	3.274(3)	Bi(6)−Se(11) ×2	2.988(2)	2.956(3)
Bi(2)−Se(6) ×2	2.866(2)	2.856(2)	Bi(7)−Se(9)	2.741(3)	2.753(3)
Bi(2)−Se(5)	2.892(3)	2.875(3)	Bi(7)−Se(12) ×2	2.772(2)	2.762(2)
Bi(2)−Se(3)	3.051(3)	3.047(3)	Bi(7)−Se(13) ×2	3.218(2)	3.227(2)
Bi(2)−Se(2) ×2	3.081(2)	3.077(2)	Bi(7)−Se(15)	3.257(3)	3.233(3)
Bi(3)−Se(7) ×2	2.900(2)	2.890(2)	Bi(8)−Se(10)	2.742(3)	2.719(3)
Bi(3)−Se(6)	2.923(3)	2.877(3)	Bi(8)−Se(13) ×2	2.910(2)	2.893(2)
Bi(3)−Se(3) ×2	3.090(2)	3.063(2)	Bi(8)−Se(14) ×2	3.017(2)	3.026(2)
Bi(3)−Se(3)	3.108(3)	3.099(3)	Bi(8)−Se(14)	3.211(3)	3.248(3)
Bi(4)−Se(8) ×2	2.917(2)	2.976(3)	Bi(9)−Se(11)	2.721(3)	2.730(3)
Bi(4)−Se(7)	2.950(3)	2.986(3)	Bi(9)−Se(15) ×2	2.811(2)	2.811(2)
Bi(4)−Se(2)	3.013(3)	2.976(2)	Bi(9)−Se(14) ×2	3.156(2)	3.159(2)
Bi(4)−Se(3) ×2	3.077(2)	3.081(2)	Bi(9)−Se(13)	3.394(3)	3.380(3)
Bi(5)−Se(8)	2.799(3)	2.791(3)	K(1)−Se(9) ×2	3.445(6)	3.408(6)
Bi(5)−Se(1) ×2	2.944(2)	2.908(2)	K(1)−Se(4) ×2	3.458(6)	3.423(6)
Bi(5)−Se(2) ×2	3.014(2)	3.007(2)	K(1)−Se(12) ×2	3.531(6)	3.546(6)
Bi(5)−Se(1)	3.376(3)	3.318(3)	K(1)−Se(12)	3.407(7)	3.432(8)
			K(1)−Se(5)	3.533(7)	3.612(8)
			K(1)−Se(15)	3.566(8)	3.582(8)
			K(2′)−Sn(2)		0.72(6)
			K(2′)−Se(6) ×2		3.20(5)
			K(2′)−Se(9) ×2		3.25(5)
			K(2′)−Se(10) ×2		3.29(5)
			K(2′)−Se(5)		3.50(6)
			K(2′)−Se(13)		3.51(6)

Table 4. Selected Distances (Å) for $K_{1.45}Pb_{3.1}Sb_{7.45}Se_{15}$ and $K_{2.15}Pb_{1.7}Sb_{8.15}Se_{15}$

	$K_{1.45}Pb_{3.1}Sb_{7.45}Se_{15}$	$K_{2.15}Pb_{1.7}Sb_{8.15}Se_{15}$		$K_{1.45}Pb_{3.1}Sb_{7.45}Se_{15}$	$K_{2.15}Pb_{1.7}Sb_{8.15}Se_{15}$
Pb(1)−Se(4) ×2	2.960(2)	2.9639(14)	Pb(2)−Se(9) ×2	2.953(2)	2.923(2)
Pb(1)−Se(15)	3.157(2)	3.163(2)	Pb(2)−Se(13)	3.012(2)	3.025(3)
Pb(1)−Se(1)	3.234(2)	3.257(2)	Pb(2)−Se(10) ×2	3.303(2)	3.379(2)
Pb(1)−Se(8) ×2	3.363(2)	3.378(2)	Pb(2)−Se(5)	3.602(2)	3.581(3)
Pb(1)−Se(11) ×2	3.362(2)	3.379(2)	Pb(2)−Se(6) ×2	3.574(2)	3.640(2)
Sb(1)−Se(4)	2.604(2)	2.599(2)	Sb(6)−Se(14)	2.861(2)	2.833(2)
Sb(1)−Se(5) ×2	2.806(2)	2.803(2)	Sb(6)−Se(10) ×2	2.943(2)	2.920(2)
Sb(1)−Se(1) ×2	3.041(2)	3.045(2)	Sb(6)−Se(11) ×2	2.950(2)	2.949(2)
Sb(1)−Se(2)	3.309(2)	3.329(2)	Sb(6)−Se(7)	2.968(3)	2.996(3)
Sb(2)−Se(6) ×2	2.811(2)	2.804(2)	Sb(7)−Se(9)	2.613(2)	2.613(2)
Sb(2)−Se(5)	2.874(2)	2.883(2)	Sb(7)−Se(12) ×2	2.730(2)	2.718(2)
Sb(2)−Se(3)	2.971(2)	2.958(2)	Sb(7)−Se(13) ×2	3.140(2)	3.155(2)
Sb(2)−Se(2) ×2	3.093(2)	3.101(2)	Sb(7)−Se(15)	3.355(2)	3.341(2)
Sb(3)−Se(7) ×2	2.791(2)	2.793(2)	Sb(8)−Se(10)	2.613(2)	2.605(2)
Sb(3)−Se(6)	2.841(3)	2.799(2)	Sb(8)−Se(13) ×2	2.874(2)	2.856(2)
Sb(3)−Se(3) ×2	3.113(2)	3.108(2)	Sb(8)−Se(14) ×2	2.948(2)	2.968(2)
Sb(3)−Se(3)	3.107(2)	3.125(2)	Sb(8)−Se(14)	3.321(2)	3.335(2)
Sb(4)−Se(2)	2.937(2)	2.923(2)	Sb(9)−Se(11)	2.609(2)	2.600(2)
Sb(4)−Se(8) ×2	2.951(2)	2.949(2)	Sb(9)−Se(15) ×2	2.740(2)	2.7394(13)
Sb(4)−Se(3) ×2	2.954(2)	2.955(2)	Sb(9)−Se(14) ×2	3.140(2)	3.134(2)
Sb(4)−Se(7)	2.967(3)	2.994(3)	Sb(9)−Se(13)	3.508(2)	3.514(2)
Sb(5)−Se(8)	2.637(2)	2.625(2)	K(1)−Se(5)	3.535(5)	3.570(5)
Sb(5)−Se(1) ×2	2.916(2)	2.917(2)	K(1)−Se(4) ×2	3.404(4)	3.406(4)
Sb(5)−Se(2) ×2	2.940(2)	2.931(2)	K(1)−Se(9) ×2	3.399(4)	3.398(4)
Sb(5)−Se(1)	3.519(3)	3.524(2)	K(1)−Se(12) ×2	3.564(4)	3.560(4)
			K(1)−Se(12)	3.439(5)	3.459(5)
			K(1)−Se(15)	3.475(5)	3.478(4)

stepped layers to form the three-dimensional structure. The tunnels form between the pillars and accommodate the alkali metal cations.

The connection points between the rods and the layers are metal atom sites of 8 coordination. These are the sites most prone to mixed occupancy with alkali metals or with different metals in the framework. For example, in β-$K_2Bi_8Se_{13}$ and $K_{2.5}Bi_{8.5}Se_{14}$, the corresponding sites exhibit mixed occupancy between Bi and K. In $A_{1+x}M_{4-2x}M'_{7+x}Se_{15}$, these sites may involve triple occupancy between A/M/M′. The remaining metal atom sites in the framework are distorted octahedra, the

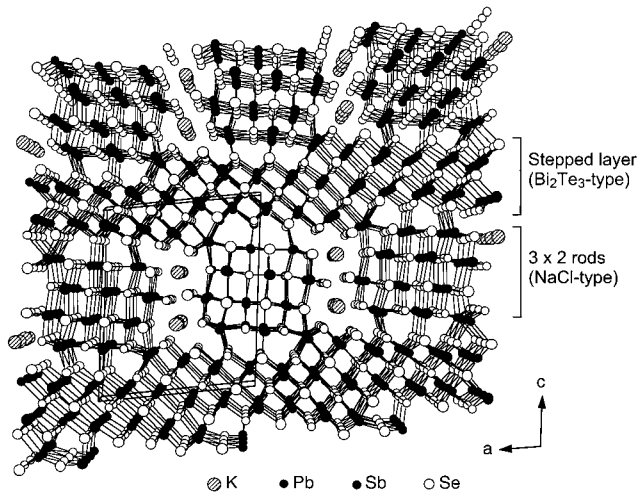

Figure 1. Structure of $K_{1.25}Pb_{3.5}Bi_{7.25}Se_{15}$ viewed down the *b* axis.

degree of distortion being subject to the identity of the metal. The distortions of the Sb octahedra found in $Rb_{1.45}Pb_{3.1}Sb_{7.45}Se_{15}$, $K_{1.45}Pb_{3.1}Sb_{7.45}Se_{15}$, and $K_{2.15}Pb_{1.7}Sb_{8.15}Se_{15}$ are more pronounced than those of Bi octahedra found in $K_{1.25}Pb_{3.5}Bi_{7.25}Se_{15}$ and $K_{1.46}Sn_{3.09}Bi_{7.45}Se_{15}$. This is due to the greater stereochemical activity of the $5s^2$ lone pair electrons of Sb^{3+} ions. In $Rb_{1.45}Pb_{3.1}Sb_{7.45}Se_{15}$, the Sb(3), Sb(4), and Sb(6) sites, which contain a considerable amount of Pb, show much milder distortions with relatively equal Sb−Se distances compared with other "clean" Sb octahedral sites. This is due to the tendency of Pb atoms to form more regular octahedral sites. Atom Se(7), which binds to Sb(3), Sb(4), and Sb(6), shows a very high ADP in all the Sb compounds. Releasing the full occupancy constraint for Se(7) did not change the occupancy, suggesting the presence of positional fluctuation. Thus, Se(7) responds to the local distortions associated with the mixed occupancy at its immediate neighbors to adjust the coordination environment of Sb or Pb. That means Se(7) displaces differently, depending on whether Sb or Pb occupies the disordered Sb(3), Sb(4), and Sb(6) sites.

The 8-coordinate sites, which are mostly occupied by Pb/Sn atoms, connect NaCl- and Bi_2Te_3-type fragments together. The Pb(1)/Sn(1) and Pb(2)/Sn(2) sites are best described as bicapped trigonal prismatic. The distortion in the Sn polyhedra is more severe than that in the Pb polyhedra because of the stereochemically more active $5s^2$ lone pair electrons of Sn^{2+} ions than $6s^2$ of Pb^{2+} ions. This pronounced stereochemical distortion due to the Sn^{2+} lone pair is also responsible for the positional disorder between Sn(2) and K(2′). This causes the Sn(2) atom to be displaced 0.72 Å away from the K(2′) atom. The Pb compound does not show any sign of positional disorder between Pb and K in these 8-coordinate sites. The ADPs for the Pb/Sn sites remain high, even after introducing mixed occupancy with alkali metal ions, indicating that either random positional fluctuation or "rattling" of the ions is occurring in these relatively spacious pockets. This condition can help the system achieve very low thermal conductivity.

The structure of $A_{1+x}M_{4-2x}M'_{7+x}Se_{15}$ is closely related to those of β-$K_2Bi_8Se_{13}$ and $K_{2.5}Bi_{8.5}Se_{14}$. The local environment of alkali metal ions and the size of the NaCl-type block in $K_{1.25}Pb_{3.50}Bi_{7.25}Se_{15}$ are also shared by β-$K_2Bi_8Se_{13}$ and $K_{2.5}Bi_{8.5}Se_{14}$; see Figure 2. Only the size of the Bi_2Te_3-type unit in each compound is different. The relationship between these three compounds can easily be seen if the formulas are broken down into two parts, the anionic framework and the alkali metal cations in the tunnels. For example, in β-$K_2Bi_8Se_{13}$, one K^+ ion is stabilized in the tunnel while the other is disordered with Bi atoms in the anionic framework as described above. Therefore, the formula can be written as $K^+[KBi_8Se_{13}]^-$ or $K^+[M_9Se_{13}]^-$ (M = K + Bi in the anionic framework). In the same way, $K_{2.5}Bi_{8.5}Se_{14}$ can be described as $K^+[M_{10}Se_{14}]^-$ and $K_{1+x}Pb_{4-2x}Bi_{7+x}Se_{15}$ as $K^+[M_{11}Se_{15}]^-$ (M = K + Bi + Pb in the anionic framework). Therefore, $K_{2.5}Bi_{8.5}Se_{14}$ and $K_{1+x}Pb_{4-2x}Bi_{7+x}Se_{15}$ are derived by successively adding neutral "MSe" units to $K_2Bi_8Se_{13}$ as follows.

$$K^+[M_9Se_{13}]^- \xrightarrow{[MSe]} K^+[M_{10}Se_{14}]^- \xrightarrow{[MSe]} K^+[M_{11}Se_{15}]^-$$

Therefore, the three compounds are members of the homologous series $K[M_{9+n}Se_{13+n}]$ in both a compositional and structural sense. This structural homology is flexible enough to preserve the basic framework through successive addition of "MSe" equivalents by adjusting the width of the Bi_2Te_3-type blocks. It would be interesting to investigate if higher order homologues predicted by the $K[M_{9+n}Se_{13+n}]$ series exist.

The modular construction of this type of compound is a major underlying characteristic and describing them in this fashion makes understanding of their structure and their interrelationships easier to achieve. The modular concept is also expected to be useful in the prediction of new compounds based on different sizes and shapes of the modules. The parent structure of course of all modules is that of NaCl.

Energy Band Gap and Thermal Analysis. The $K_{1+x}M_{4-2x}Bi_{7+x}Se_{15}$ (M = Pb, Sn) and $A_{1+x}Pb_{4-2x}Sb_{7+x}Se_{15}$ (A = K, Rb) compounds are valence precise and are narrow gap semiconductors. The band gap was easily detectable spectroscopically in the infrared region as well-defined absorption. A typical absorption spectrum revealing the energy gap of $K_{1.25}Pb_{3.5}Bi_{7.25}Se_{15}$ is shown in Figure 3. The band gaps vary from 0.35 to 0.60 eV, depending on the compound, and they are summarized in Table 5. The size of the band gap is critical to the electrical characteristic of a potential thermoelectric material. To be viable for near room-temperature applications, a material needs to have E_g of < 0.55 eV, although a correct band gap in and of itself is not a sufficient property.[23] Certainly, the band gaps observed for most members of this family lie in the desirable range.

DTA experiments indicate that they are thermodynamically stable compounds melting congruently in the narrow region between 570 and 690 °C, see Table 5 for details.

Charge Transport Properties. The charge transport properties of $K_{1.25}Pb_{3.50}Bi_{7.25}Se_{15}$ were measured on single-crystal samples. The conductivity of $K_{1.25}Pb_{3.50}Bi_{7.25}Se_{15}$ was ∼260 S/cm at room temperature and showed a metal-like trend increasing with falling temperature; however, it reaches a maximum at 50 K and

(23) Mahan, G. *J. Appl. Phys.* **1989**, *65*, 1578−1583.

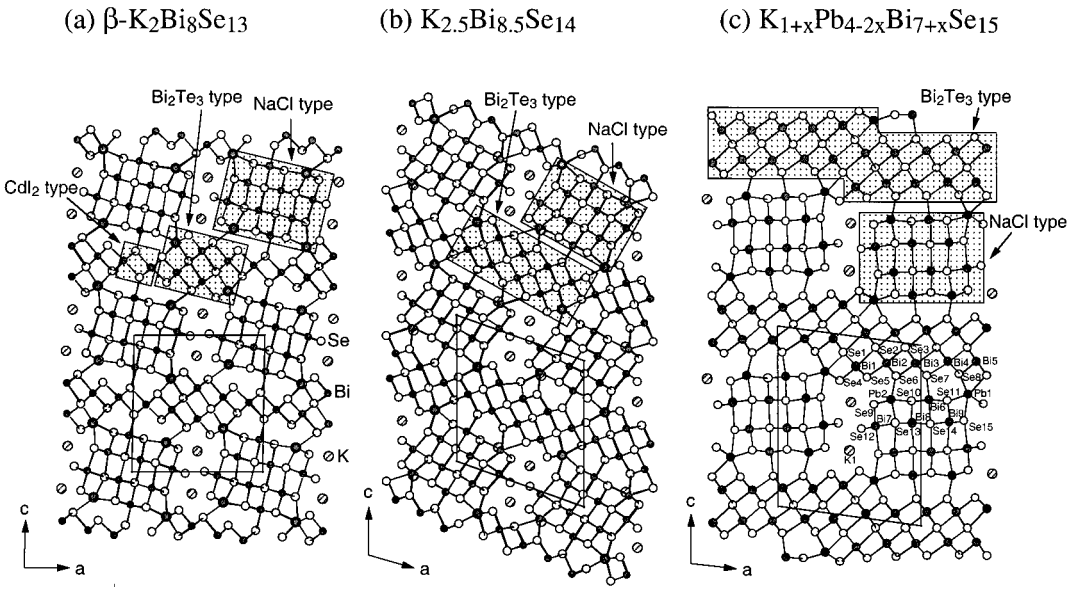

Figure 2. Structure of (a) β-$K_2Bi_8Se_{13}$, (b) $K_{2.5}Bi_{8.5}Se_{14}$, and (c) $K_{1.25}Pb_{3.5}Bi_{7.25}Se_{15}$ viewed down the *b* axis. In each case, NaCl-, Bi_2Te_3-, and CdI_2-type fragments found on the framework are shown as highlighted by the shaded areas.

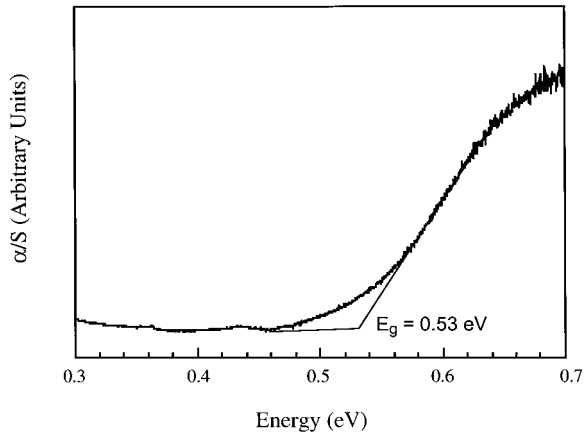

Figure 3. Optical absorption spectrum of $K_{1.25}Pb_{3.5}Bi_{7.25}Se_{15}$. The semiconductor energy gap is indicated in the spectrum.

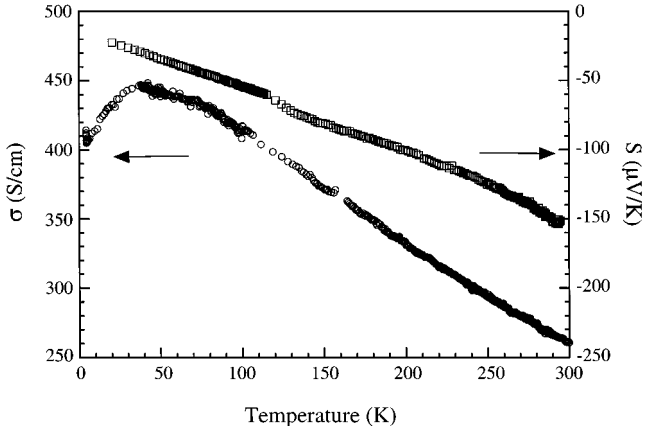

Figure 4. Variable temperature electrical conductivity and thermopower for a single crystal of $K_{1.25}Pb_{3.5}Bi_{7.25}Se_{15}$.

Table 5. Energy Band Gap, Melting Point, and Room-Temperature Charge Transport Properties

compound	E_g (RT) (eV)	mp (°C)	σ_{RT} (S/cm)	S_{RT} (μV/K)	power factor (μW/cm·K^2)
$K_{1.25}Pb_{3.50}Bi_{7.25}Se_{15}$	0.53	685	260	−150	5.85
$Rb_{1.45}Pb_{3.1}Sb_{7.45}Se_{15}$	0.36	578	1.7×10^{-2}	1331	0.03
$K_{1.45}Pb_{3.1}Sb_{7.45}Se_{15}$	0.45	576	2.6×10^{-3}	1029	2.8×10^{-3}
$K_{2.15}Pb_{1.7}Sb_{8.15}Se_{15}$	0.60	576	1.2×10^{-3}	1071	1.4×10^{-3}
$K_{1.46}Sn_{3.09}Bi_{7.45}Se_{15}$	0.39	662	110	−70	0.54

subsequently decreases, see Figure 4. The observed temperature dependence might be due to carrier localization at low temperatures associated with defects acting as traps. $K_{1.25}Pb_{3.50}Bi_{7.25}Se_{15}$ shows quite large negative Seebeck coefficients, −150 μV/K, at room temperature. The negative sign indicates that charge carriers are electrons (n-type). The excess carrier electrons could be due to a slight excess of Se atoms occupying Bi sites in the structure. The Seebeck coefficient increases almost linearly with increasing temperature starting from a value of −20 μV/K at 20 K. This temperature dependence suggests much higher Seebeck values than −150 μV/K are expected at >300 K and implies that the maximum *ZT* for this material lies above room temperature. The charge transport properties are highly dependent on the degree of doping. Varying degrees of doping can be achieved in several ways, including adding impurities deliberately or changing the synthetic conditions. For example, ingot samples of this compound prepared with a different method than that for single crystals exhibit different values of electrical conductivity and thermopower (see below). Systematic doping studies will be reported elsewhere.

The room-temperature electrical conductivity of an ingot of $K_{1.46}Sn_{3.09}Bi_{7.45}Se_{15}$ was found to be ~110 S/cm. Thermopower measurements reveal n-type behavior with a room-temperature Seebeck coefficient of −70 μV/K, see Figure 5. The thermopower increases at higher temperatures to −120 μV/K at 400 K.

The charge transport properties of the Sb phases were measured on single-crystal samples. They exhibit semiconducting behavior with room-temperature conductivities of 1.7×10^{-2}, 2.6×10^{-3}, and 1.2×10^{-3} S/cm for $Rb_{1.45}Pb_{3.1}Sb_{7.45}Se_{15}$, $K_{1.45}Pb_{3.1}Sb_{7.45}Se_{15}$, and $K_{2.15}Pb_{1.7}Sb_{8.15}Se_{15}$, respectively, see Figure 6. These values are too low for TE applications. Unlike $K_{1.25}Pb_{3.50}Bi_{7.25}Se_{15}$, the Sb phases are doped p-type and possess enormous room-temperature thermopower of 1331, 1029, and 1071

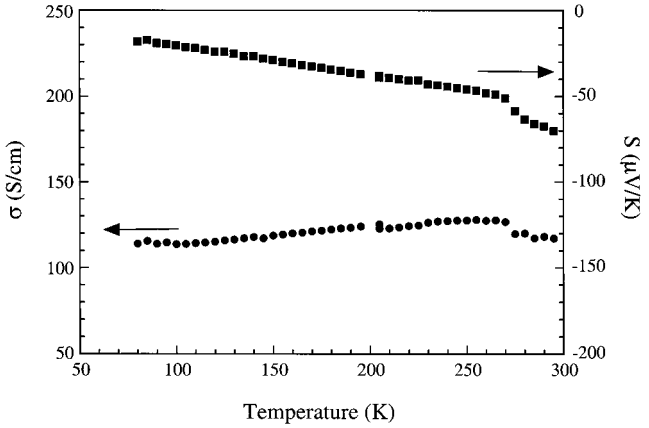

Figure 5. Variable temperature electrical conductivity and thermopower for an ingot of $K_{1.46}Sn_{3.09}Bi_{7.45}Se_{15}$.

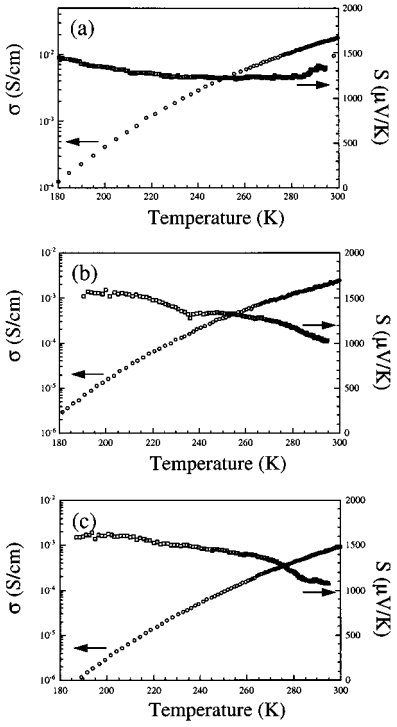

Figure 6. Variable temperature electrical conductivity and thermopower for a single crystal of (a) $Rb_{1.45}Pb_{3.1}Sb_{7.45}Se_{15}$, (b) $K_{1.45}Pb_{3.1}Sb_{7.45}Se_{15}$, and (c) $K_{2.15}Pb_{1.7}Sb_{8.15}Se_{15}$.

μV/K for $Rb_{1.45}Pb_{3.1}Sb_{7.45}Se_{15}$, $K_{1.45}Pb_{3.1}Sb_{7.45}Se_{15}$, and $K_{2.15}Pb_{1.7}Sb_{8.15}Se_{15}$, respectively, consistent with their very low electrical conductivity values. $K_{1.45}Pb_{3.1}Sb_{7.45}Se_{15}$with a higher Pb content shows higher electrical conductivity than $K_{2.15}Pb_{1.7}Sb_{8.15}Se_{15}$ with comparable thermopower (Figure 6). We speculate that the origin of holes in these systems could be due to a slight amount of Sb atom substitution of Se sites in the structure.

Thermal Conductivity. Unfortunately, it was not possible to measure the thermal conductivity of small single crystals. For this measurement, large ingots of the material are required, and therefore only the thermal transport properties of $K_{1.25}Pb_{3.50}Bi_{7.25}Se_{15}$ were measured using elongated ingots (approximately 2 × 2 × 5 mm). The ingot was prepared by melting a stoichiometric mixture of K_2Se, Pb, Bi, and Se metals in a carbon-coated silica tube. Because of the different preparation methods, doping levels of such ingots are usually different from those of the single crystals discussed above. For example, the ingot thus prepared exhibited a much higher electrical conductivity of ~800 S/cm and lower thermopower of −25 μV/K at room temperature, see Figure 7. Therefore, the "as-made" ingot samples are heavily doped with a larger number of carriers than the single-crystal samples.

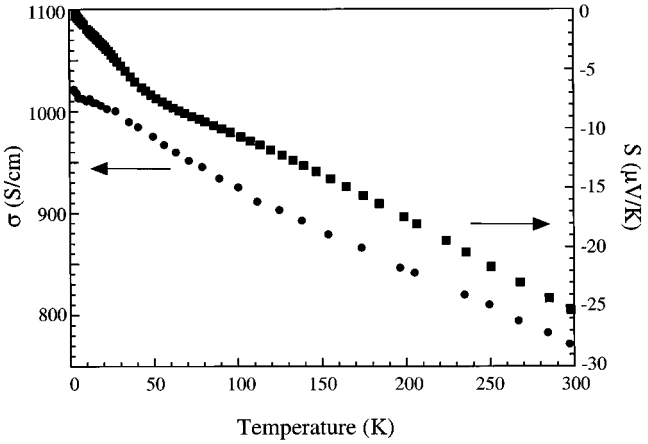

Figure 7. Variable temperature electrical conductivity and thermopower for a polycrystalline ingot of $K_{1.25}Pb_{3.5}Bi_{7.25}Se_{15}$.

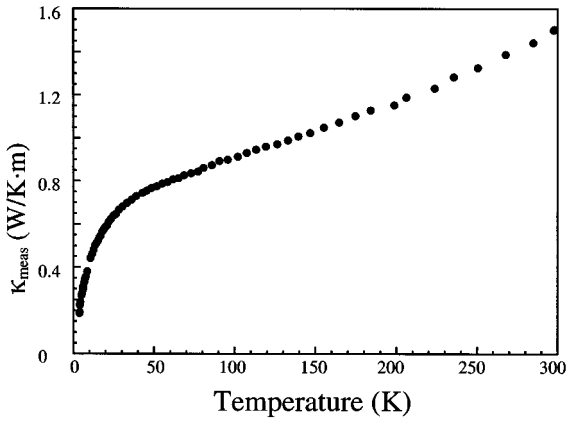

Figure 8. Variable temperature thermal conductivity, κ_{meas}, for an ingot of $K_{1.25}Pb_{3.5}Bi_{7.25}Se_{15}$.

Heating the stoichiometrically combined elements seems to produce more defects in the ingot sample, perhaps antisite and/or Se vacancies that generate more carriers. In contrast, the flux method, used to prepare the single crystals, provides a Se-rich medium that discourages Se vacancies. At the same time the slow crystal growth conditions reduce the number of antisite defects and keep the doping level of the material relatively low. The doping effects associated with this material and their dependence on preparation conditions will be investigated further in the future.

The thermal conductivity, κ_{meas}, of $K_{1.25}Pb_{3.50}Bi_{7.25}Se_{15}$ measured along the needle axis (i.e., *b* axis) of an oriented ingot is shown in Figure 8. The room-temperature κ_{meas} value is very low at ~1.50 W/m·K, and it is comparable to that of the optimized $Bi_2Te_{3-x}Se_x$ alloy, which is ~1.5 W/m·K.[24] Given that the electronic contribution, which is calculated from the electrical

(24) Encyclopedia of Materials Science and Engineering; *Thermoelectric Semiconductors*; MIT Press: Cambridge, MA; Pergamon Press: Oxford, 1986; p 4968.

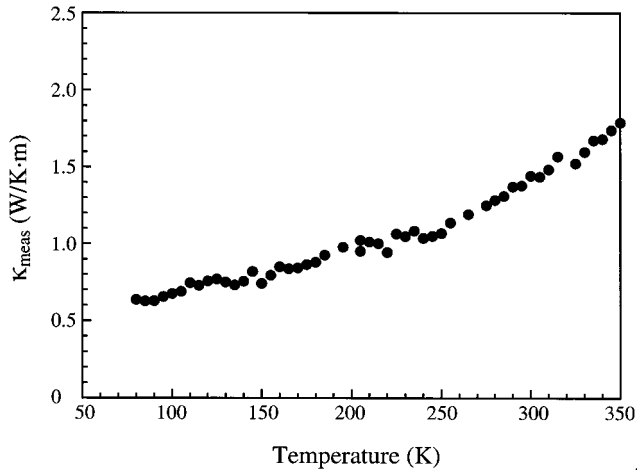

Figure 9. Variable temperature thermal conductivity, κ_{meas}, for an ingot of $K_{1.46}Sn_{3.09}Bi_{7.45}Se_{15}$.

conductivity data using the Wiedemann−Franz law,[25] is 0.56 W/m·K, the lattice contribution, κ_{latt}, is estimated to be only ∼0.94 W/m·K at room temperature.

The structural and compositional complexity, the rattling effect of alkali metal and Pb^{2+} ions in cavities, and the alloy-type occupancy disorder among the K, Pb, and Bi atoms in $K_{1.25}Pb_{3.50}Bi_{7.25}Se_{15}$ all combine to produce a very low lattice thermal conductivity indeed. At this point the figure of merit (ZT) for the single crystals of $K_{1.25}Pb_{3.50}Bi_{7.25}Se_{15}$ is estimated to be ∼0.2 at room temperature. The ZT of pure Bi_2Te_3 is 0.5 and the optimized Bi_2Te_3 alloy is ∼0.9. Despite this, a ZT ∼ 0.2 is high enough to suggest that $K_{1.25}Pb_{3.50}Bi_{7.25}Se_{15}$ be considered as a viable candidate for thermoelectric research that warrants serious experimental efforts at ZT optimization.

The thermal conductivity of $K_{1.46}Sn_{3.09}Bi_{7.45}Se_{15}$ was also measured on polycrystalline ingots, see Figure 9. The room-temperature κ_{meas} was ∼1.44 W/m·K (uncorrected for radiative losses), again a very low value due to the same reasons discussed above. The thermal conductivity shows very similar temperature dependence to that of $K_{1.25}Pb_{3.50}Bi_{7.25}Se_{15}$. It gradually increases as the temperature rises and the rapid increase above 250 K is due to the enhanced contribution of radiative loss at higher temperature.

(25) Kittel, C. *Introduction to Solid State Physics*, 6th ed.; John Wiley & Sons, Inc.: New York, 1986; p 150.

4. Concluding Remarks

The general formula $A_{1+x}M_{4-2x}M'_{7+x}Se_{15}$ (A = K, Rb; M = Pb, Sn; M′ = Bi, Sb) represents a large flexible family of stable materials. The flexibility comes from the ability to vary x and to substitute a large number of group 1, group 14, and group 15 atoms. The adopted structure type is novel and related to those of β-$K_2Bi_8Se_{13}$ and $K_{2.5}Bi_{8.5}Se_{14}$. The $K_{1.25}Pb_{3.50}Bi_{7.25}Se_{15}$ member is a potential thermoelectric material because it possesses a favorable combination of enhanced electrical and thermal transport properties. The complexity of the structure with its selected sites exhibiting mixed occupancy of K/Pb/Bi atoms creates a system in which heat flow is significantly frustrated. Consequently, this system possesses one of the lowest thermal conductivities reported for crystalline materials. This work demonstrates that, in contrast to simpler high-symmetry binary compounds, it is not only possible but actually straightforward to achieve very low thermal conductivity in quaternary chalcogenide compounds as long as they possess complex compositions and structures. The fact that Sb and Sn analogues of $K_{1.25}Pb_{3.5}Bi_{7.25}Se_{15}$ exist should enhance the ability to optimize the TE properties by making systematic Bi−Sb or Pb−Sn solid solution studies possible, without substantially disrupting the structure.

Acknowledgment. Financial support from the Office of Naval Research (Grant N00014-98-1-0443) is gratefully acknowledged. Work at Northwestern University made use of the Central Facilities supported by the National Science Foundation though the Northwestern University Materials Research Center (DMR-9632472).

Supporting Information Available: Tables of crystallographic details, atomic coordinates, and isotropic and anisotropic displacement parameters for all atoms for $K_{1.25}Pb_{3.5}Bi_{7.25}Se_{15}$, $Rb_{1.45}Pb_{3.1}Sb_{7.45}Se_{15}$, $K_{1.45}Pb_{3.1}Sb_{7.45}Se_{15}$, $K_{2.15}Pb_{1.7}Sb_{8.15}Se_{15}$, and $K_{1.46}Sn_{3.09}Bi_{7.45}Se_{15}$ (PDF). This material is available free of charge via the Internet at http://pubs.acs.org.

CM0003323